Springer

Journal of Mechanical Science and Technology 23 (2009) 2138~2148

Journal of Mechanical Science and Technology

www.springerlink.com/content/1738-494x
DOI 10.1007/s12206-009-0502-5

Research on transmission paths of a coupled beam-cylindrical shell system by power flow analysis †

G. P. Feng*, Z. Y. Zhang, Y. Chen and H. X. Hua

State Key Laboratory of Mechanical System and Vibration, Shanghai Jiao Tong University, Shanghai 200240, China

(Manuscript Received October 21, 2008; Revised March 18, 2009; Accepted April 10, 2009)

Abstract

A power flow analysis based on a substructure approach is performed to exhibit vibration transmission in a complex coupled beam-cylindrical shell system. The system is divided into a shell substructure and a beam substructure, which are coupled by three spring-dampers. The theoretical receptance function of each substructure with a free-free interface condition is formulated by modal analysis to describe the dynamical behavior. On the basis of the receptance functions of the two substructures as well as synthesis through the geometrical compatibility and force balance conditions at the coupling interfaces, the dynamic characteristics of the coupled system are calculated. Both the input and transmitted powers within the system are estimated, and the influences of the excitation locations, the stiffness and loss factor of the spring-dampers on the vibration transmission are investigated as well.

Keywords: Vibration power flow; Substructure approach; Receptance; Transmission

1. Introduction

During navigation the engine and propeller will excite hull structures through the shaft and bearings. The induced stern vibrations and sound transmission are potential threats for submarines. Hence, it is important to reduce the vibration level of the stern.

Over the past few decades, most work has been conducted to investigate the characteristics of the hull and propeller shafting system of a submarine. Ruotolo [1] compared various shell theories in computing the natural frequencies of cylinders stiffened with rings and stringers, where the effect of stiffeners was considered. The influence of external fluid loading on the dynamic response of fluid-filled cylindrical shells was also investigated [2, 3]. Ross [2] used the finite element and boundary element techniques to obtain the natural frequencies of a submerged cylindrical shell. Merz et al. [4] discussed the far-field radiated sound pressure of a submerged cylinder through an analytical formulation.

In addition, Wang and Daley [5] examined the active control at the propeller shafting system and found that it is possible to design a controller to reduce vibration levels of both the thrust block and the propeller. Goodwin [6] investigated the reduction of excessive vibration in the propeller shafting system by using a hydraulic device known as a resonance changer. In his study, a simple spring-mass model of the propeller shafting system is used and the coupling between the shafting system and the hull is not considered. By using the resonance changer, Dylejko [7-8] further studied the vibration transmission in marine vessels, and the dynamic response of the propeller shafting system is exhibited, where the hull is modeled as a one-dimensional rod for an initial approximation.

Most work has investigated the submarine hull and the propeller shafting system. However, few researches have taken into account the coupling be-

† This paper was recommended for publication in revised form by Associate Editor Eung-Soo Shin

*Corresponding author. Tel.: +86 21 3420 6664, Fax.: +86 21 3420 6813
E-mail address: f_gp@sjtu.edu.cn

tween them. The stern is a complicated structure, which consists of hulls, shaft, propeller and engine. To control the vibration, it is apparently insufficient to only investigate the characteristics of hulls and the shafting system, respectively. Therefore, the stern or the submarine is necessarily regarded as a whole system, considering the coupling effects between hulls and the shafting system.

To reduce the vibration and noise level, it is a good practice to isolate transmitted vibration power flows from the sources. Understanding the power flow from a vibration source to other parts of a structure, and the reduction of its transmission is of practical interest. Hence, it is necessary to quantify not only the vibration level but also the transmission of vibration energy in the structures. One way to determining vibration energy transmission is by conducting a power flow analysis (PFA).

Power flow analysis is very useful for the measurement of vibration energy injected or transmitted into structures and for controlling of noise and vibration in industries. This method can be successfully used for identification and ranking of transmission paths of vibration power flow in structures. It is not possible to obtain enough information by experimental modal analysis as it generally deals with the modal parameters such as mode shapes, loss factors and natural frequencies to characterize the vibration of a built up structure. As a result, this method can practically be used in industries for noise and vibration control, giving a guide to isolation of vibration sources as well as damping treatments to most energy transfer surfaces in the structures.

The fundamental concept of power flow was proposed by Noiseux [9] and Pavic [10] in the early 1970s, aiming to develop measurement techniques of power flow for simple structural elements. Noiseux measured the vibration intensity in uniform plates and beams vibrating in flexure. Recently, this approach has been further developed and used widely to model complex structures [11, 12], access vibration control systems [13-15] and identify damage of structures [18-20]. Cuschieri [11] used a mobility method to analyze the power flow in L-plates. Lu and Wang [13] studied the structure-borne vibration power flow transmission for a steel construction parking tower. Xiong et al. [14] developed progressive approaches to PFA and applied them to a complex coupled floating raft vibration isolation system. In addition, the concept of a power flow density vector developed by Xing and Price [16, 17] was further investigated. The magnitude and direction of the power flow density vector at any location of the structure were calculated and used to identify the damage location [18-20]. Lee et al. [19] calculated the diversion of energy flow near crack tips of a vibrating plate, showing that a crack can be identified by the changes of the directions of intensity vectors near the crack. Wong [20] studied the power flow and energy distribution of a vibration mode of a damaged plate, and found that the modal power flow is effective and more sensitive for damage identification.

For complex structures, finite element analysis [21-23] (FEA) is often used to analyze the dynamic behavior with good accuracy in the low-frequency range. Jenkinseta [21] used a finite element model to demonstrate the detailed dynamics of a typical raft-isolation-receiver system using secondary force inputs in parallel with a passive isolation system. Qu and Selvam [22] developed dynamic condensation method to reduce the number of degrees of freedom of finite element models for a damped system. Xu [23] investigated the intensity of a rectangular plate with stiffeners using the finite element method. The finite element method can conveniently model structures with complex boundary conditions. However, in general, it is necessary to adopt a large number of modes into an analysis to ensure the convergence of solution. In this circumstance, FEA encounters difficulties due to the required computation load. To overcome this disadvantage, Wang et al. [24] proposed a substructure method to analyze the power flow, where the complex system is divided into many substructures and the dynamic responses of the structure are obtained efficiently by analytical methods.

In this paper, the submarine stern is simplified to a beam-cylindrical shell system. The vibration transmission in the system is investigated by using the power flow analysis. In Section 2, the theoretical receptance function of each substructure with a free-free interface condition is formulated by modal analysis to describe the dynamic behavior of each substructure. The input and transmission power flow formulas are presented in Section 3. In Section 4, influences of the excitation locations, stiffness and loss factor of the spring-dampers on the power flow transmission characteristics are investigated by simulation.

2. Substructure approach

As shown in Fig. 1, the submarine stern consists of hulls, shaft, propeller, engine and so on, and the shaft and hulls are coupled by three bearing links. In general, the hulls are modeled as cylindrical shells since a more detailed modeling of hulls has very little effect, as reported by Merz et al. [4]. Hence, in this analysis, the stern is simplified to a beam-cylindrical shell system. The hull and the shaft are modeled as a cylindrical shell and a beam, respectively. They are coupled by three spring-dampers, standing for the bearing links between the hull and the shaft. The coupled system is excited at the two ends of the beam to simulate the exciting forces of the propeller and the engine, respectively. The beam-cylindrical shell system is illustrated in Fig. 2. By the substructure approach, the system can be separated into two subsystems. In this section, the theoretical receptance function of each substructure with a free-free interface condition is formulated by modal analysis to describe the dynamic behavior.

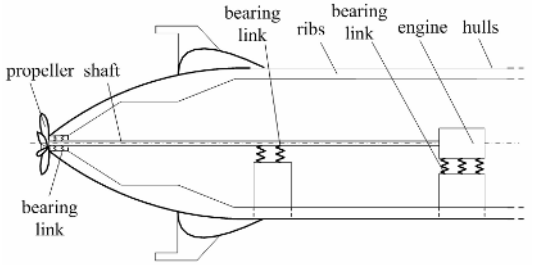

Fig. 1. Schematic illustration of a submarine stern.

2.1 Vibration of the cylindrical shell

As shown in Figs. 2(b) and 2(c), the shaft and hull are treated as a single uniform beam and a uniform cylindrical shell, respectively. In the figure, R is the radius of the cylindrical shell, h the thickness and $h/R << 1$. u, v and w are displacements of the cylindrical shell in the axial, tangential and radial directions, respectively. F_x, F_ϕ and F_r denote the exciting forces in the corresponding three directions. Under the assumption of thin shell theory [25], the differential equations describing the dynamic behavior are expressed as

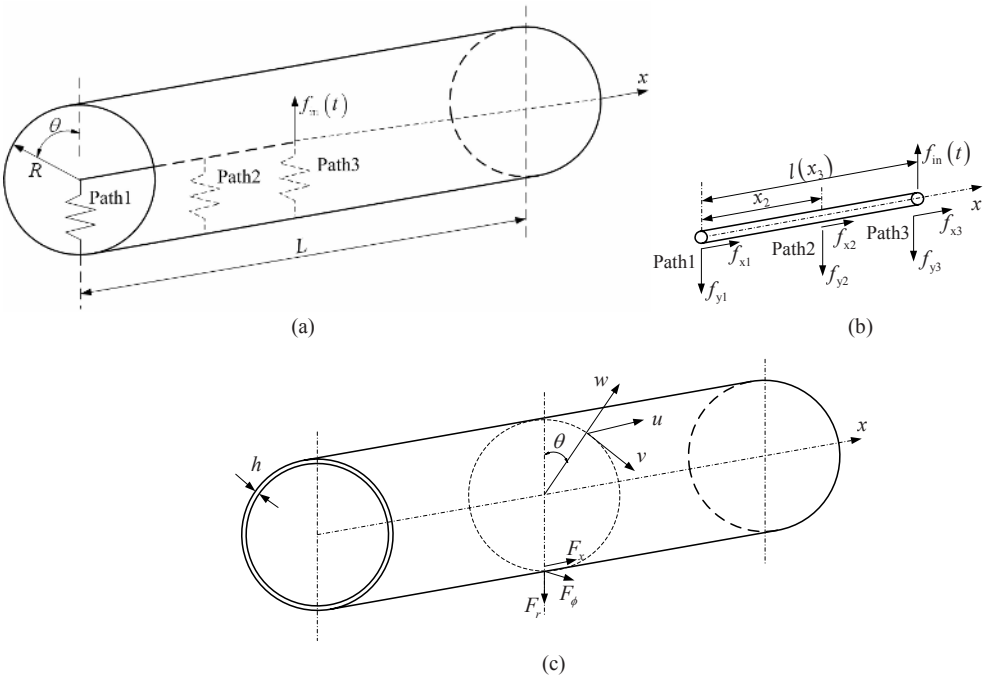

Fig. 2. Schematic illustration of a beam-cylindrical shell system. (a) the system, (b) the beam, (c) the cylindrical shell.

$$\frac{\partial^2 u}{\partial x^2}+\frac{1-\mu}{2R^2}\frac{\partial^2 u}{\partial \phi^2}+\frac{1+\mu}{2R}\frac{\partial^2 v}{\partial x\partial \phi}+\frac{\mu}{R}\frac{\partial w}{\partial x}-\frac{1}{c_P^2}\frac{\partial^2 u}{\partial t^2}=\frac{-F_x}{\rho_P h c_P^2}$$

$$\frac{1}{R^2}\frac{\partial^2 v}{\partial \phi^2}+\frac{1-\mu}{2}\frac{\partial^2 v}{\partial x^2}+\frac{1+\mu}{2R}\frac{\partial^2 u}{\partial x\partial \phi}+\frac{1}{R^2}\frac{\partial w}{\partial \phi}-\frac{1}{c_P^2}\frac{\partial^2 v}{\partial t^2}=\frac{-F_\phi}{\rho_P h c_P^2}$$

$$\beta^2\left(R^2\frac{\partial^4 w}{\partial x^4}+\frac{2\partial^4 w}{\partial x^2\partial \phi^2}+\frac{1}{R^2}\frac{\partial^4 w}{\partial \phi^4}\right)+\frac{\mu}{R}\frac{\partial u}{\partial x}$$

$$+\frac{1}{R^2}\frac{\partial v}{\partial \phi}+\frac{w}{R^2}+\frac{1}{c_P^2}\frac{\partial^2 w}{\partial t^2}=\frac{F_r}{\rho_P h c_P^2} \quad (1)$$

where μ and ρ_P are the Poisson ratio and density of the shell, respectively, c_P the phase velocity of the compressional wave travelling in the elastic shell, given by $c_P=\left[E/\rho_P\left(1-\mu^2\right)\right]^{1/2}$. $\beta^2=h^2/12R^2$ the effect of bending stress.

It is assumed that the cylindrical shell is simply supported. Based on the modal superposition method, displacements u, v, w are expressed as

$$u(\phi,x)=\sum_{\alpha=0}^{1}\sum_{n=0}^{\infty}\sum_{m=1}^{\infty}U_{mn}^{\alpha}\sin\left(n\phi+\frac{\alpha\pi}{2}\right)\cos k_m x e^{jwt}$$

$$v(\phi,x)=\sum_{\alpha=0}^{1}\sum_{n=0}^{\infty}\sum_{m=1}^{\infty}V_{mn}^{\alpha}\cos\left(n\phi+\frac{\alpha\pi}{2}\right)\sin k_m x e^{jwt} \quad (2)$$

$$w(\phi,x)=\sum_{\alpha=0}^{1}\sum_{n=0}^{\infty}\sum_{m=1}^{\infty}W_{mn}^{\alpha}\sin\left(n\phi+\frac{\alpha\pi}{2}\right)\sin k_m x e^{jwt}$$

In the same way, the forces acting on the shell can be written as

$$F_{xmn}^{\alpha}=\frac{2}{\pi L}F_x(x,\phi)\sin\left(n\phi+\frac{\alpha\pi}{2}\right)\cos k_m x$$

$$F_{\phi mn}^{\alpha}=\frac{2}{\pi L}F_\phi(x,\phi)\cos\left(n\phi+\frac{\alpha\pi}{2}\right)\sin k_m x \quad (3)$$

$$F_{rmn}^{\alpha}=\frac{2}{\pi L}F_r(x,\phi)\sin\left(n\phi+\frac{\alpha\pi}{2}\right)\sin k_m x$$

where $j^2=-1$, $\alpha=0,1$ denote the symmetric and asymmetric vibrations in the circumferential director, respectively. $k_m=m\pi/L$ is the axial mode number depending on the boundary conditions of the cylindrical shell.

Substitution of Eqs.(2) and (3) into Eq.(1) yields the following matrix form of the relationship between $\left\{U_{mn}^{\alpha}\quad V_{mn}^{\alpha}\quad W_{mn}^{\alpha}\right\}$ and $\left\{F_{xmn}^{\alpha}\quad F_{\phi mn}^{\alpha}\quad F_{rmn}^{\alpha}\right\}$

$$\begin{bmatrix}L_{11}&L_{12}&L_{13}\\L_{21}&L_{22}&L_{23}\\L_{31}&L_{32}&L_{33}\end{bmatrix}\begin{bmatrix}U_{mn}^{\alpha}\\V_{mn}^{\alpha}\\W_{mn}^{\alpha}\end{bmatrix}=\frac{1-\mu^2}{Eh}\begin{bmatrix}F_{xmn}^{\alpha}\\F_{\phi mn}^{\alpha}\\F_{rmn}^{\alpha}\end{bmatrix} \quad (4)$$

Where

$$L_{11}=k_m^2+\frac{1}{2R^2}(1-\mu)n^2-\Omega^2,$$

$$L_{12}=L_{21}=\frac{1}{2R}(1+\mu)nk_m,\ L_{13}=L_{31}=-\frac{\mu k_m}{R},$$

$$L_{22}=\frac{1}{2}(1-\mu)k_m+\frac{n^2}{R^2}-\Omega^2,\ L_{23}=L_{32}=-\frac{n}{R^2},$$

$$L_{33}=\beta^2\left(Rk_m{}^2+\frac{n^2}{R}\right)^2+\frac{1}{R^2}-\Omega^2,$$

$\Omega=\omega/c_P$ is the non-dimensional frequency.

By definition

$$\begin{bmatrix}L_{11}&L_{12}&L_{13}\\L_{21}&L_{22}&L_{23}\\L_{31}&L_{32}&L_{33}\end{bmatrix}=[L] \quad (5)$$

$[L]=0$ is the characteristic equation of the cylindrical shell. From Eq. (4), receptance functions of the shell can be derived easily. For example, when the shell is excited only by a normal force, the receptance function is

$$Z_{mn}=\frac{W_{mn}^{\alpha}(k_m)}{F_{rmn}^{\alpha}(k_m)}=\frac{1-\mu^2}{Eh}\frac{L_{11}L_{22}-L_{12}L_{21}}{|L|}$$

Based on these results, the responses of the cylindrical shell represented by Eq. (2) can be determined under any kind of excitation. The applied forces F_x, F_ϕ and F_r in Eq.(1) consist of internal coupling forces. For this linear system, it is convenient to express the displacements U_{mn}^{α}, V_{mn}^{α} and W_{mn}^{α} described by Eqs. (2) and (4). Therefore, the displacements of the shell at three coupling points are represented as follows:

$$\boldsymbol{U}_{\mathrm{cs}}=\boldsymbol{S}_{\mathrm{c}}\boldsymbol{F}_{\mathrm{cs}},\ \boldsymbol{U}_{\mathrm{cs}}=\begin{bmatrix}u\\v\\w\end{bmatrix} \quad (6)$$

where $\boldsymbol{S}_{\mathrm{c}}$ denotes the interface receptance function matrix of the shell under internal coupling forces $\boldsymbol{F}_{\mathrm{cs}}$. These receptance functions, representing the displacement response vectors to each unit internal coupling force, are determined. The internal coupling force $\boldsymbol{F}_{\mathrm{cs}}$ remains unknown and needs to be determined by undertaking a synthesis process using geometrical compatibility conditions and force balance equations at the cou-

pling points, which is described in Sections 2.2 and 2.3.

2.2 Vibration of the beam

For a straight beam, it is assumed that the axial and lateral motions are uncoupled. The differential equations of the axial and lateral motions of the beam as shown in Fig. 2(b) are expressed as

$$-EI(1+i\eta)\frac{\partial^4 w}{\partial x^4}+\rho A\frac{\partial^2 w}{\partial t^2}=f_{\text{in}}+\sum_i f_{yi}\delta(l-x_i)$$

$$-EA(1+i\eta)\frac{\partial^2 u}{\partial x^2}+\rho A\frac{\partial^2 u}{\partial t^2}=\sum_i f_{xi}\delta(l-x_i)$$

where u, w are displacements of the beam in the axial and transverse directions, respectively. f_x, f_y denote the exciting forces in the axial and transverse directions, respectively. l is the length of the beam and x_i denote the location of paths.

According to modal superposition theory, the responses can be written as

$$w(x,t)=\sum_{i=1}^{\infty}\phi_i(x)q_i(t),\quad u(x,t)=\sum_{i=1}^{\infty}\varphi_i(x)p_i(t)$$

where ϕ_i, φ_i denote the mode shapes associated with the axial and lateral vibration of the beam, respectively. Moreover, q_i and p_i represent the corresponding principal coordinates.

The displacements of the beam under the internal coupling forces and external excitations have a similar matrix form, given as follows:

$$\boldsymbol{U}_{\text{cb}}=\boldsymbol{R}_{\text{c}}\boldsymbol{F}_{\text{cb}}+\boldsymbol{R}_{\text{e}}\boldsymbol{F}_{\text{e}},\quad \boldsymbol{U}_{\text{cb}}=\begin{bmatrix}u\\ w\end{bmatrix} \tag{7}$$

where $\boldsymbol{R}_{\text{c}}$, $\boldsymbol{R}_{\text{e}}$ denote the interface receptance functions of the beam corresponding to the internal coupling force $\boldsymbol{F}_{\text{cb}}$ and external excitation $\boldsymbol{F}_{\text{e}}$, respectively.

2.3 Synthesis of substructures

The substructures are connected by spring-dampers, which are massless and have different constant complex stiffness at the coupling points. Therefore, the complex stiffness matrix at any position in the global coordinate system can be written as

$$\boldsymbol{K}=\begin{Bmatrix}K_x(1+i\eta_x)\\ K_y(1+i\eta_y)\end{Bmatrix}$$

In this coupled system, there are three spring-dampers. Accordingly, Eqs. (6) and (7) are extended into

$$\begin{bmatrix}\boldsymbol{U}_{\text{cs}}^{(1)}\\ \boldsymbol{U}_{\text{cs}}^{(2)}\\ \boldsymbol{U}_{\text{cs}}^{(3)}\end{bmatrix}=\begin{bmatrix}\boldsymbol{S}_{\text{c}}^{11} & \boldsymbol{S}_{\text{c}}^{12} & \boldsymbol{S}_{\text{c}}^{13}\\ \boldsymbol{S}_{\text{c}}^{21} & \boldsymbol{S}_{\text{c}}^{22} & \boldsymbol{S}_{\text{c}}^{23}\\ \boldsymbol{S}_{\text{c}}^{31} & \boldsymbol{S}_{\text{c}}^{32} & \boldsymbol{S}_{\text{c}}^{33}\end{bmatrix}\cdot\begin{bmatrix}\boldsymbol{F}_{\text{cs}}^{(1)}\\ \boldsymbol{F}_{\text{cs}}^{(2)}\\ \boldsymbol{F}_{\text{cs}}^{(3)}\end{bmatrix} \tag{8}$$

$$\begin{bmatrix}\boldsymbol{U}_{\text{cb}}^{(1)}\\ \boldsymbol{U}_{\text{cb}}^{(2)}\\ \boldsymbol{U}_{\text{cb}}^{(3)}\end{bmatrix}=\begin{bmatrix}\boldsymbol{R}_{\text{c}}^{11} & \boldsymbol{R}_{\text{c}}^{12} & \boldsymbol{R}_{\text{c}}^{13}\\ \boldsymbol{R}_{\text{c}}^{21} & \boldsymbol{R}_{\text{c}}^{22} & \boldsymbol{R}_{\text{c}}^{23}\\ \boldsymbol{R}_{\text{c}}^{31} & \boldsymbol{R}_{\text{c}}^{32} & \boldsymbol{R}_{\text{c}}^{33}\end{bmatrix}\cdot\begin{bmatrix}\boldsymbol{F}_{\text{cb}}^{(1)}\\ \boldsymbol{F}_{\text{cb}}^{(2)}\\ \boldsymbol{F}_{\text{cb}}^{(3)}\end{bmatrix}+\begin{bmatrix}\boldsymbol{R}_{\text{e}}^{1}\boldsymbol{F}_{\text{e}}\\ \boldsymbol{R}_{\text{e}}^{2}\boldsymbol{F}_{\text{e}}\\ \boldsymbol{R}_{\text{e}}^{3}\boldsymbol{F}_{\text{e}}\end{bmatrix} \tag{9}$$

The coupling conditions of the two substructures are described by the force balance and geometric compatibility. In the global coordinate system, these conditions at three couplings are expressed as follows:

$$\begin{bmatrix}\boldsymbol{T}_{\text{b}}\boldsymbol{F}_{\text{cb}}^{(1)}\\ \boldsymbol{T}_{\text{b}}\boldsymbol{F}_{\text{cb}}^{(2)}\\ \boldsymbol{T}_{\text{b}}\boldsymbol{F}_{\text{cb}}^{(3)}\end{bmatrix}=\begin{bmatrix}\boldsymbol{K}_1\left(\boldsymbol{T}_{\text{s1}}\boldsymbol{U}_{\text{cs}}^{(1)}-\boldsymbol{T}_{\text{b}}\boldsymbol{U}_{\text{cb}}^{(1)}\right)\\ \boldsymbol{K}_2\left(\boldsymbol{T}_{\text{s2}}\boldsymbol{U}_{\text{cs}}^{(2)}-\boldsymbol{T}_{\text{b}}\boldsymbol{U}_{\text{cb}}^{(2)}\right)\\ \boldsymbol{K}_3\left(\boldsymbol{T}_{\text{s3}}\boldsymbol{U}_{\text{cs}}^{(3)}-\boldsymbol{T}_{\text{b}}\boldsymbol{U}_{\text{cb}}^{(3)}\right)\end{bmatrix}=\begin{bmatrix}\boldsymbol{T}_{\text{b}}\boldsymbol{F}_{\text{cb}}^{(1)}\\ \boldsymbol{T}_{\text{b}}\boldsymbol{F}_{\text{cb}}^{(2)}\\ \boldsymbol{T}_{\text{b}}\boldsymbol{F}_{\text{cb}}^{(3)}\end{bmatrix}=-\begin{bmatrix}\boldsymbol{T}_{\text{s1}}\boldsymbol{F}_{\text{cs}}^{(1)}\\ \boldsymbol{T}_{\text{s2}}\boldsymbol{F}_{\text{cs}}^{(2)}\\ \boldsymbol{T}_{\text{s3}}\boldsymbol{F}_{\text{cs}}^{(3)}\end{bmatrix} \tag{10}$$

where $\boldsymbol{T}_b$ is the transformation matrix connecting the local beam coordinate system and the global coordinate system. $\boldsymbol{T}_{\text{s1}}$, $\boldsymbol{T}_{\text{s2}}$ and $\boldsymbol{T}_{\text{s3}}$ are the transformation matrices from the local shell coordinate systems to the global coordinate system, defined at three couplings, respectively.

Substituting Eqs. (8) and (9) to Eq. (10), the coupling conditions become

$$\begin{bmatrix}\boldsymbol{T}_{\text{b}}\boldsymbol{F}_{\text{cb}}^{(1)}\\ \boldsymbol{T}_{\text{b}}\boldsymbol{F}_{\text{cb}}^{(2)}\\ \boldsymbol{T}_{\text{b}}\boldsymbol{F}_{\text{cb}}^{(3)}\end{bmatrix}=-[\boldsymbol{K}]\left\{\left([\boldsymbol{R}_{\text{c}}]+[\boldsymbol{S}_{\text{c}}]\right)\begin{bmatrix}\boldsymbol{T}_{\text{b}}\boldsymbol{F}_{\text{cb}}^{(1)}\\ \boldsymbol{T}_{\text{b}}\boldsymbol{F}_{\text{cb}}^{(2)}\\ \boldsymbol{T}_{\text{b}}\boldsymbol{F}_{\text{cb}}^{(3)}\end{bmatrix}+\begin{bmatrix}\boldsymbol{T}_{\text{b}}\boldsymbol{R}_{\text{e}}^{1}\boldsymbol{F}_{\text{e}}\\ \boldsymbol{T}_{\text{b}}\boldsymbol{R}_{\text{e}}^{2}\boldsymbol{F}_{\text{e}}\\ \boldsymbol{T}_{\text{b}}\boldsymbol{R}_{\text{e}}^{3}\boldsymbol{F}_{\text{e}}\end{bmatrix}\right\}$$

where

$$[\boldsymbol{K}]=\begin{bmatrix}\boldsymbol{K}_1 & & \\ & \boldsymbol{K}_2 & \\ & & \boldsymbol{K}_3\end{bmatrix}[\boldsymbol{R}_{\text{c}}]=\begin{bmatrix}\boldsymbol{T}_{\text{b}}\boldsymbol{R}_{\text{c}}^{11}\boldsymbol{T}_{\text{b}}^{-1} & \boldsymbol{T}_{\text{b}}\boldsymbol{R}_{\text{c}}^{12}\boldsymbol{T}_{\text{b}}^{-1} & \boldsymbol{T}_{\text{b}}\boldsymbol{R}_{\text{c}}^{13}\boldsymbol{T}_{\text{b}}^{-1}\\ \boldsymbol{T}_{\text{b}}\boldsymbol{R}_{\text{c}}^{21}\boldsymbol{T}_{\text{b}}^{-1} & \boldsymbol{T}_{\text{b}}\boldsymbol{R}_{\text{c}}^{22}\boldsymbol{T}_{\text{b}}^{-1} & \boldsymbol{T}_{\text{b}}\boldsymbol{R}_{\text{c}}^{23}\boldsymbol{T}_{\text{b}}^{-1}\\ \boldsymbol{T}_{\text{b}}\boldsymbol{R}_{\text{c}}^{31}\boldsymbol{T}_{\text{b}}^{-1} & \boldsymbol{T}_{\text{b}}\boldsymbol{R}_{\text{c}}^{32}\boldsymbol{T}_{\text{b}}^{-1} & \boldsymbol{T}_{\text{b}}\boldsymbol{R}_{\text{c}}^{33}\boldsymbol{T}_{\text{b}}^{-1}\end{bmatrix}$$

$$[\boldsymbol{S}_{\mathrm{c}}]=\begin{bmatrix} \boldsymbol{T}_{\mathrm{s1}}\boldsymbol{S}_{\mathrm{c}}^{11}\boldsymbol{T}_{\mathrm{s1}}^{-1} & \boldsymbol{T}_{\mathrm{s1}}\boldsymbol{S}_{\mathrm{c}}^{12}\boldsymbol{T}_{\mathrm{s2}}^{-1} & \boldsymbol{T}_{\mathrm{s1}}\boldsymbol{S}_{\mathrm{c}}^{13}\boldsymbol{T}_{\mathrm{s3}}^{-1} \\ \boldsymbol{T}_{\mathrm{s2}}\boldsymbol{S}_{\mathrm{c}}^{21}\boldsymbol{T}_{\mathrm{s1}}^{-1} & \boldsymbol{T}_{\mathrm{s2}}\boldsymbol{S}_{\mathrm{c}}^{22}\boldsymbol{T}_{\mathrm{s2}}^{-1} & \boldsymbol{T}_{\mathrm{s2}}\boldsymbol{S}_{\mathrm{c}}^{23}\boldsymbol{T}_{\mathrm{s3}}^{-1} \\ \boldsymbol{T}_{\mathrm{s3}}\boldsymbol{S}_{\mathrm{c}}^{31}\boldsymbol{T}_{\mathrm{s1}}^{-1} & \boldsymbol{T}_{\mathrm{s3}}\boldsymbol{S}_{\mathrm{c}}^{32}\boldsymbol{T}_{\mathrm{s2}}^{-1} & \boldsymbol{T}_{\mathrm{s3}}\boldsymbol{S}_{\mathrm{c}}^{33}\boldsymbol{T}_{\mathrm{s3}}^{-1} \end{bmatrix}.$$

Hence, the coupling forces in the global coordinate system are now written as

$$\begin{bmatrix} \boldsymbol{T}_{\mathrm{b}}\boldsymbol{F}_{\mathrm{cb}}^{(1)} \\ \boldsymbol{T}_{\mathrm{b}}\boldsymbol{F}_{\mathrm{cb}}^{(2)} \\ \boldsymbol{T}_{\mathrm{b}}\boldsymbol{F}_{\mathrm{cb}}^{(3)} \end{bmatrix}=-\left([\boldsymbol{I}]+[\boldsymbol{K}][\boldsymbol{S}_{\mathrm{c}}]+[\boldsymbol{K}][\boldsymbol{R}_{\mathrm{c}}]\right)^{-1}[\boldsymbol{K}]\begin{bmatrix} \boldsymbol{T}_{\mathrm{b}}\boldsymbol{R}_{\mathrm{e}}^{1}\boldsymbol{F}_{\mathrm{e}} \\ \boldsymbol{T}_{\mathrm{b}}\boldsymbol{R}_{\mathrm{e}}^{2}\boldsymbol{F}_{\mathrm{e}} \\ \boldsymbol{T}_{\mathrm{b}}\boldsymbol{R}_{\mathrm{e}}^{3}\boldsymbol{F}_{\mathrm{e}} \end{bmatrix}$$

3. Power flow analysis

The instantaneous mechanical power at point i is defined as [9-12]

$$P(t)=f_i(t)v_i(t)$$

where $f_i(t)$ is the internal force and $v_i(t)$ the velocity at the point of interest. For vibrating structures the time averaged power flow is defined by

$$\langle P(t)\rangle=\frac{1}{T}\int_0^T f_i(t)v_i(t)dt$$

where the symbol $\langle\ \rangle$ represents the temporal average. In the frequency domain, the time averaged power flow can be calculated by

$$\langle P\rangle=\frac{1}{2}\mathrm{Re}\left\{f_i v_i^*\right\}$$

where the symbol $*$ represents the complex conjugate, Re represents the real part, f_i and v_i are the internal force and the point velocity response, respectively, at a given frequency.

Thus, the input power flow and transmitted power flow from the beam to the shell can be formulated as follows:

$$\langle P_{\mathrm{in}}\rangle=\frac{1}{2}\mathrm{Re}\left\{f_{\mathrm{in}}\,\dot{u}^*\right\}$$

$$\left\langle P_{\mathrm{trans}}^{(j)}\right\rangle=\frac{1}{2}\mathrm{Re}\left\{\left(\boldsymbol{F}_{\mathrm{cb}}^{(j)}\right)^{\mathrm{T}}\left(\dot{\boldsymbol{U}}_{\mathrm{cb}}^{(j)}\right)^{*}\right\}\quad j=1,2,3$$

4. Numerical results

In this section, the input power flow of external excitation and transmitted power flows from the beam to the cylindrical shell through various paths are calculated through numerical simulations. Moreover, the influences of the excitation locations, the stiffness and loss factor of the spring-dampers on the vibration transmission are investigated.

To validate our work, the input and transmitted power flows out of the above substructure approach are first compared with those from the finite element analysis method. The parameters of the beam-cylindrical shell system shown in Fig. 2 are listed in Table 1. Three uniform spring-dampers are set between the beam and the cylindrical shell. The complex stiffness of the spring-damper is only in the y direction and defined by

$K=K_0\left(1+\mathrm{i}\eta_{\mathrm{y}}\right)\mathrm{N/m^2}$ $K_0=5\times10^6\mathrm{N/m^2}$

The loss factor is chosen to be zero and a unit amplitude excitation is applied at one end of the beam (at Path 1).

Fig. 3 shows the predictions of the transmitted power flow through Path 3 by the two methods. It is observed that the results derived by both the FEA and theoretical approach have a good agreement although there is small difference in the higher frequency range, which is possibly caused by adopting a small number of modes in the FEA approach. Therefore, the presented theoretical

Table 1. Parameters of the beam-cylindrical shell system.

Parameter	Value
Yong's modulus E (GPa)	2.1×10^{11}
Poisson's ratio μ	0.3
Loss factor η	0.01
Density of beam ρ (Kg/m^3)	7800
Length of beam L_{b} (m)	1.5
Section area A (m^2)	2.5×10^{-4}
Inertia moment I (Kg$\cdot$m^2)	6.2×10^{-7}
Shell thickness h (m)	0.006
Density of shell ρ_{p} (Kg/m^3)	7800
Radius of shell R (m)	0.75
Length of shell L (m)	3

Table 2. Main parameters of the spring-dampers.

	Stiffness K	Loss factor η_{y}
Case 1	$0.1K_0$	0
Case 2	K_0	
Case 3	$10K_0$	
Case 4(2)	K_0	0
Case 5		0.01
Case 6		0.1

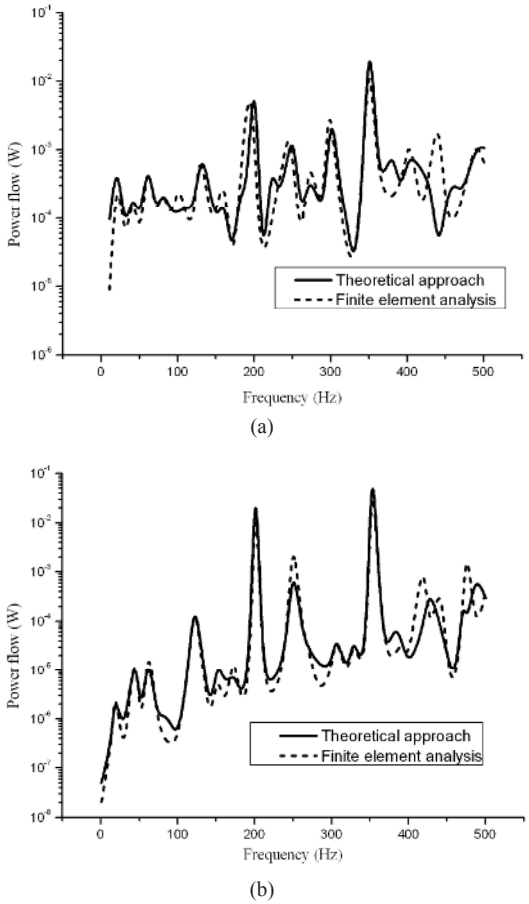

Fig. 3. Predictions of input power and transmitted power by Path 3. (a) input power, (b) transmitted power.

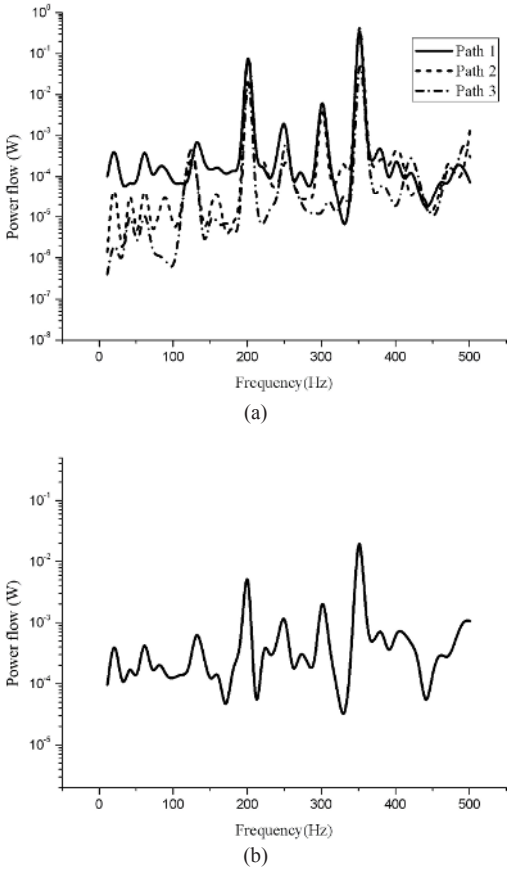

Fig. 4. Predictions of transmitted power through three paths and input power at Path 1. (a) transmitted power, (b) input power.

method has a good accuracy in the low to medium frequency range for analysis of the beam-cylindrical shell system.

Next, the influence of the excitation location on the vibration transmission is revealed. Figures 4(a) and 4(b) illustrate the time-averaged input power of an external force at Path 1(one end of the beam) and the transmitted power through the three paths from the beam to the shell. From Fig. 4, it can be seen that Path 1 is dominant in power transmission compared with the other two. When the external force excites at Path 3 (another end of the beam), the transmitted power through the three paths are shown in Fig. 5 (a). It can be seen that Path 3 is dominant. In Fig. 5 (b), the input powers of both external forces are represented.

From Figs. 4 and 5, it is found that the location of excitation force will affect power transmission paths. The path near the excitation location through which the transmitted power is larger is dominant. Fig. 5(b) illustrates that the input powers are different when excitation is at different locations although the external forces are of the same magnitude. Moreover, it shows the whole system can receive higher input power when excited at the stern under the same conditions.

The effect of the spring-dampers on power transmission paths is exhibited by using different stiffness and loss factor. The parameters of the spring-dampers are listed in Table 2 and Table 1. The external force is a unit harmonic point force at Path 3 in those cases.

The effect of the stiffness of the spring-dampers on power transmission paths is shown in Figs. 6, 7 and 8, and the effect on input power in the three cases is represented in Fig. 9. From Figs. 6-8, it is found that increasing the stiffness of the spring-dampers makes Path 3 dominant in case 1 and case 2. From Fig. 9, it can be inferred that stiffening the spring-dampers reduces the input power at high frequencies. This can be interpreted as that the displacement of the beams is larger when the

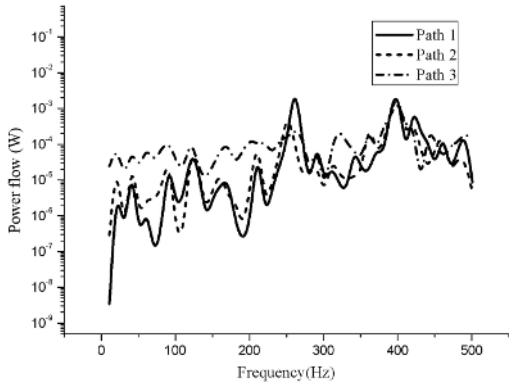

(a)

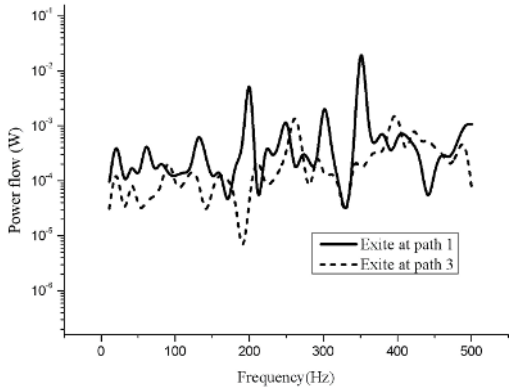

(b)

Fig. 5. Predictions of transmitted power through three paths and input power at Path 3. (a) transmitted power, (b) input power in comparison with Fig.2(b).

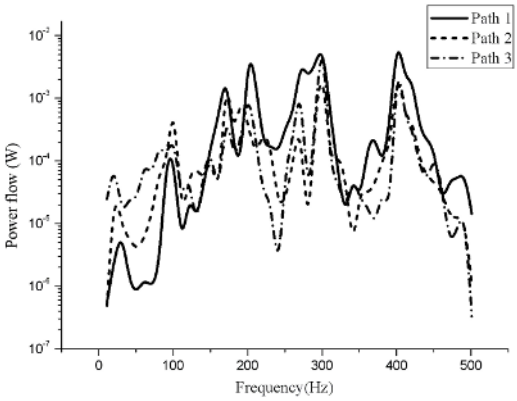

Fig. 6. Predictions of transmitted power through three paths in case 1.

stiffness is softer. Accordingly, the input power becomes small.

Further, the effect of the loss factor of the spring-dampers on power transmission is investigated. The

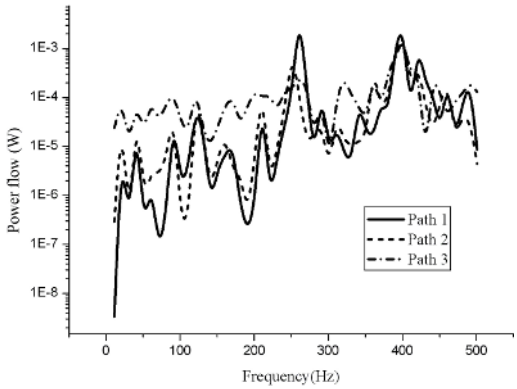

Fig. 7. Predictions of transmitted power through three paths in case 2(4).

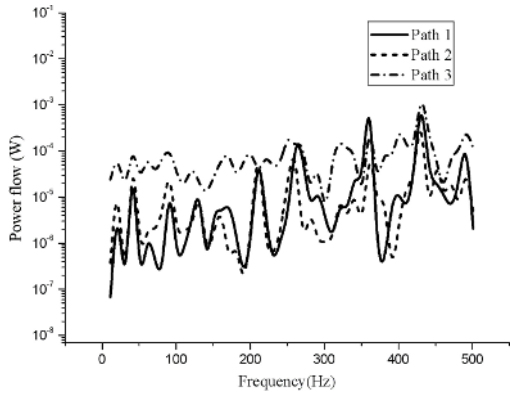

Fig. 8. Predictions of transmitted power through three paths in case 3.

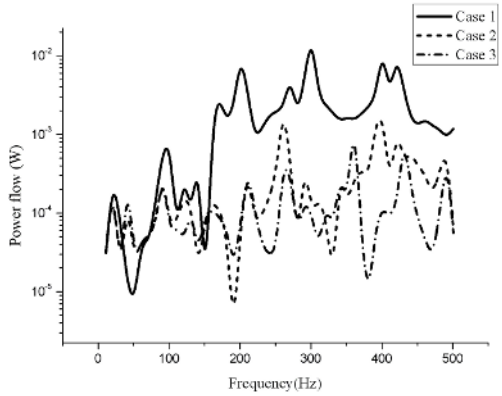

Fig. 9. Predictions of input power in three cases 1-3.

results are shown in Figs. 7, 10 and 11 with predictions of time-averaged transmitted power through three paths in cases 4, 5 and 6. The effect on input power is represented in Fig. 12 for the three cases.

From Figs. 7, 10 and 11, it is observed that in case

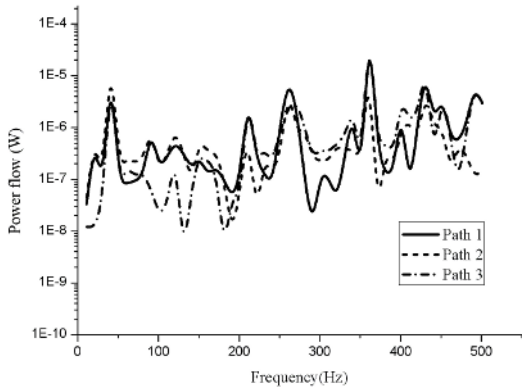

Fig. 10. Predictions of transmitted power through three paths in case 5.

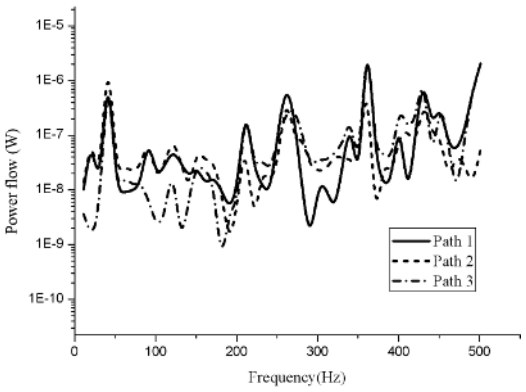

Fig. 11. Predictions of transmitted power through three paths in case 6.

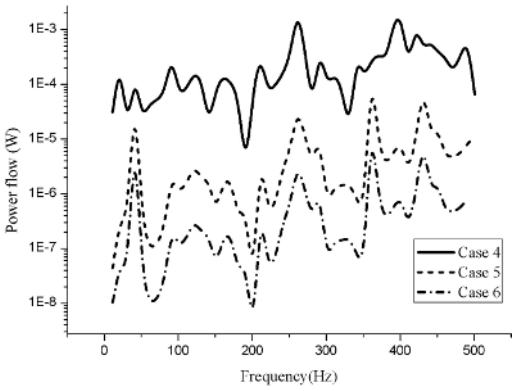

Fig. 12. Predictions of input power in the cases 4, 5, 6.

4 where the damping ratio is zero, Path 3 is significant compared to other paths. In case 2 as well as case 3, Path 3 is not significant at lower frequencies but dominant at higher frequencies. That is, a damper can change the vibration transmission path of the system. This result is interesting and further investigation is necessary for a better understanding. Nevertheless, we are reminded that the proper design of the spring-damper may effectively control the vibration of the system.

In Fig. 12, it can be inferred that increasing damping of the spring-damper system reduces the input power rapidly, and the natural frequencies remain unchanged when the damping factor is small.

5. Conclusions

Discussed in this paper is the vibration transmission of a submarine stern that is simplified into a coupled beam-cylindrical shell system. Structural vibration transmission paths have been analyzed by using the substructure method. The results show that vibration transmission is closely related to the installation locations as well as the stiffness and damping of the spring-dampers. The total injected or transmitted power is dependent on the natural frequencies of the structure. The path near the location of the external force is dominant. In addition, vibration transmission paths can be changed by softening or stiffening the spring-dampers. Increasing damping will reduce the input power flow, although the transmission power may be not related to damping.

In fact, there are many decks and stiffened plates that have a certain influence on vibration transmission in a submarine. It seems simple to simplify the submarine stern without taking into account the effects of the decks and stiffened plates. Regardless of the limitation, this study does suggest that an optimized design/modification or vibration control for a coupled beam-cylindrical system can be obtained based on the power flow analysis.

References

[1] R. Ruotolo, A comparison of some thin shell theories used for the dynamic analysis of stiffened cylinders, *Journal of Sound and Vibration*, 243 (2001) 847-860.

[2] C. T. F. Ross, P. Haynes and W. D. Richards, Vibration of ring-stiffened circular cylinders under external water pressure, *Computers and Structures*, 60 (1996) 1013-1019.

[3] G. C. Everstine, Prediction of low frequency vibrational frequencies of submerged structures, *Journal of Vibration and Acoustics, Transactions of the ASME*, 113 (1991) 187-191.

[4] S. Merz, S. Oberst, P. G. Dylejko et al., Development of coupled FE/BE models to investigate the structural and acoustic responses of a submerged vessel, *Journal of Computational Acoustics*, 15 (2007) 23-47.

[5] J. Wang and S. Daley, A geometric approach to the optimal design of remotely located broadband vibration control systems, *Proceedings of the 14th International Congress on Sound and Vibration*, Cairns, Australia, (2007) 9-12.

[6] A. J. H. Goodwin, The design of a resonance changer to overcome excessive axial vibration of propeller shafting, *Transactions of the Institute of Marine Engineers*, **7**2 (1960) 37-63.

[7] P. G. Dylejko and N. J. Kessissoglou, Minimization of vibration transmission through the propeller-shafting system in a submarine, *Journal of the Acoustical Society of America* (A), 116 (4) (2004) 2569.

[8] P. G. Dylejko, N. J. Kessissoglou, Y. K. Tso et al., Optimisation of a resonance changer to minimise the vibration transmission in marine vessels, *Journal of Sound and Vibration*, 300 (2007) 101-116.

[9] D. U. Noiseux, Measurement of power flow in uniform beams and plates, *Journal of the Acoustical Society of America*, 47 (1970) 238-247.

[10] G. Pavic, Measurement of structure borne wave intensity, part I: formulation of the methods, *Journal of Sound and Vibration*, 49 (1) (1976) 221-230.

[11] J. M. Cuschieri, Vibration transmission through periodic structures using a mobility power flow approach, *Journal of Sound and Vibration*, 143 (1) (1990) 65-74.

[12] M. F. M. Hussein and H. E. M. Hunt, A power flow method for evaluating vibration from underground railways, *Journal of Sound and Vibration*, 293 (3-5) (2006) 667-679.

[13] W. Y. Lu and W. H. Wang, Diagnosis and control of machine induced noise and vibration in steel construction, *Journal of Mechanical Science and Technology*, 22 (11) (2008) 2107-2121.

[14] Y. P. Xiong, J. T. Xing and W. G. Price, Power flow analysis of complex coupled systems by progressive approaches, *Journal of Sound and Vibration*, 239 (2) (2001) 275-295.

[15] W. J. Choi, Y. P. Xiong and R. A. Shenoi, Power flow analysis for a floating sandwich raft isolation system using a higher-order theory, *Journal of Sound and Vibration*, 319 (2009) 228-246.

[16] J. T. Xing and W. G. Price, A power-flow analysis based on continuum dynamics, *Proceedings of the Royal Society* A, 455 (1999) 401-436.

[17] J. T. Xing, W. G. Price and Z. H. Wang, A study of power flow characteristics using a vector field analysis approach, in: H. Hu (Editor-in-chief), *Proceedings of the Fifth International Conference on Vibration Engineering*, China Aviation Industry Press, Beijing (2002) 33-40

[18] M. S. Khun, H. P. Lee and S. P. Lim, Structural intensity in plates with multiple discrete and distributed spring-dashpot systems, *Journal of Sound and Vibration*, 276 (2004) 627-648.

[19] H. P. Lee, S. P. Lim and M. S. Khun, Diversion of energy flow near crack tips of a vibrating plate using the structural intensity technique, *Journal of Sound and Vibration*, 296 (2006) 602-622.

[20] W. O. Wong, X. Q. Wang and L. Cheng, Modal power flow analysis of a damaged plate, *Journal of Sound and Vibration*, 320 (2009) 84-100.

[21] M. D. Jenkins, P. A. Nelson, R. J. Pinnington and S. J. Elliott, Active isolation of periodic machinery vibrations, *Journal of Sound and Vibration*, 166 (1) (1993) 117-140.

[22] Z. Q. Qu and R. P. Selvam, Efficient method for dynamic condensation of nonclassically damped vibrations sytems, *AIAA Journal*, 40 (2) (2002) 368-375.

[23] X. D. Xu, H. P. Lee and C. Lu, Power flow paths in stiffened plates, *Journal of Sound and Vibration*, 282 (3-5) (2005) 1264-1272.

[24] Z. H. Wang, J. T. Xing and W. G. Price, An investigation of power flow characteristics of L-shaped plates adopting a substructure approach, *Journal of Sound and Vibration*, 250 (4) (2002) 627-648.

[25] M. C. Junger and D. Feit, *Sound, Structures and Their Interaction*, MIT Press, Cambridge, MA (1986).

G.P. Feng received his Ph.D. from the School of Mechanical Engineering at Shanghai Jiao Tong University. His research interests include vibration analysis, control and sound radiation, etc.

Z.Y. Zhang received his Ph.D. from the School of Mechanical Engineering at Shanghai Jiao Tong University. Dr. Zhang is currently a Professor at the School of Mechanical Engineering at Shanghai Jiao Tong University in Shanghai, China.

Y. Chen received his Ph.D. from the School of Mechanical Engineering at Shanghai Jiao Tong University. His research interests include vibration and shock analysis.

H.X. Hua received his Ph.D. at the University of Brussels in Belgium. Dr. Hua is currently a Professor and Doctoral Supervisor at the School of Mechanical Engineering at Shanghai Jiao Tong University in Shanghai, China. His research interests include modal parameter identification, and analysis of vibration and shock.